RESEARCH ARTICLE

Characteristics of isolated hybrid tremor (HBT) during a calm activity period at Aso Volcano

Takehiko Mori · Yasuaki Sudo · Tomoki Tsutsui · Shin Yoshikawa

Abstract Isolated-type tremors having two events with different dominant frequencies are characteristic seismological phenomena observed during the fumarolic activity stage at Aso Volcano. These isolated tremors are called hybrid tremors (HBT) and comprise two parts: an initial part named the "HF-part" with a dominant frequency in the high-frequency region (approximately 10 Hz) and the following part named the "LF-part" with a dominant frequency in the low-frequency region (approximately 2 Hz). The LF-part is observed after the HF-part, and the HBT is accompanied by a long-period tremor (LPT). Hypocenters and source parameters are estimated using seismograms recorded at 64 stations around Nakadake crater. The amplitude distributions of all HF-parts have almost similar trends. Similarly, the amplitude distributions of all LF-parts have almost similar trends. However, the amplitude distributions of HF- and LF-parts are not similar. From these results, we proposed that the hypocenters and source parameters of HF- and LF-parts are not common, but each of them have common hypocenters and source parameters. The hypocenter region of HF-parts was estimated to be just beneath the fumarole region south of the 1st crater: the volume fluctuation is the major source factor. The hypocenter region of LF-parts is estimated to be at a depth of approximately 300 m beneath the first crater: the strike–slip component is the major source parameter. The hypocentral depth of LF-parts is located at the upper end of the crack estimated to be the source of the LPTs. The LPTs and HBTs are observed almost simultaneously. We consider that volcanic fluid is involved in the source mechanisms of both HBT and LPT.

T. Mori (✉)
Geological Survey of Japan, National Institute of Advanced Industrial Science and Technology,
1-1-1 Higashi, Tsukuba,
Ibaraki, Japan
e-mail: mori.may0212@aist.go.jp

Y. Sudo
The Foundation of Aso Volcano Museum,
1930-1 Akamizu, Aso,
Kumamoto, Japan

T. Tsutsui
Faculty of Engineering and Resource Science, Akita University,
1-1 Tegatagakuen, Akita,
Akita, Japan

S. Yoshikawa
Aso Volcanological Laboratory, Graduate School of Science,
Kyoto University,
5280 Kawayô, Minamiaso,
Kumamoto, Japan

Introduction

A seismological phenomenon called a volcanic tremor has been observed since the beginning of seismic observations near active volcanoes or craters before and after many volcanic eruptions: many studies about hypocenters and source mechanisms have been performed. Volcanic tremors have been classified according to the frequency characteristics or durations of the observed seismograms (e.g., Seidl et al. 1990; Hurst 1992; Miller et al. 1998). Advancements in seismometer designs have brought about new knowledge about volcanic tremors; for example, broadband seismometers have clarified the existence of long-period volcanic

tremors with a dominant period exceeding 10 s (e.g., Kawakatsu et al. 1992). Studies on the source mechanisms of long-period volcanic tremors compared to short-period ones have seen progress in the past several years (e.g., Chouet et al. 1999; Yamamoto et al. 1999b; Legrand et al. 2000). The study of the source mechanisms of long-period volcanic tremors is comparatively easy because the waveforms of these tremors are not influenced by the heterogeneity of the volcanic edifice. In contrast, short-period volcanic tremors with a short wavelength are subjected to large attenuation and scattering effects for heterogeneity. To obtain waveforms of the short-period volcanic tremors without being influenced by various effects, it is necessary to place instruments near an active crater and set many observation points or develop array observations.

Aso Volcano in Japan is one of the volcanoes where it is easy to approach the active crater. There is a roadway to the crater rim, and tourists can visit the crater rim using a car. Volcanological observations using various techniques have been performed near the active crater (e.g., Tanaka 1994; Mori and Notsu 1997; Yamamoto et al. 1999b; Hase et al. 2005). In 1998, we deployed a dense seismic network near the active crater of Aso Volcano and observed the short-period volcanic tremor with a duration of several seconds, which is called an isolated-type tremor. In this paper, we estimate hypocenter regions and source parameters of this volcanic tremor and discuss its relationship with the volcanic activity in Aso Volcano.

Activity of Aso Volcano

Aso Volcano is located in central Kyushu, Japan and comprises several central cones located inside a large caldera (Ono and Watanabe 1985). In recent years, among the central cones of Aso Volcano, only Nakadake crater (with seven craters) has been active. Explosive eruptions occurred in four craters (first, second, third, and fourth crater) of Nakadake in the 1920s and 1930s (Japan Meteorological Agency 2005). After this period, eruptions have occurred only in the first crater, and continuous fumarolic activities have been observed in the south wall of the first crater. When the volcanic activity is calm, the first crater is filled with hot water, and the burst of air bubbles or a very small-scale ejection of gases is sometimes observed at the surface of the center of the crater lake. When this activity level increases, the ejection of gases from the surface of the crater lake becomes larger and more frequent and the water level in the crater lake decreases with the activity of the phreatic explosions. After the crater lake dries up, ash often erupts, and the active stage steps forward to Strombolian eruptions. The last Strombolian eruption occurred in 1993. Although phreatic explosions occurred in 1994, 1995, and 2004, the first crater was always filled by the crater lake after 1993.

High emission rates of volcanic gases have been continuously observed even when the crater lake is present (e.g., the SO_2 emission rate measured by Mori et al. (2006) was approximately 4 kg/s). A continuous activity of volcanic gas emission suggests that Aso Volcano has a shallow magmatic activity at all the times.

History of seismic observations

In the 1930s when the explosive eruptions repeated, seismic observations in Aso Volcano were initiated. Sassa (1935) classified the volcanic seismic signals from Aso Volcano into four different kinds of volcanic tremors and "eruption earthquakes". These classifications are "the volcanic microtremors of the first kind" (a dominant period of 0.8–1.5 s), "the second kind" (3.5–8.0 s), "the third kind" (0.4–0.6 s), and "the fourth kind" (0.2 s). Thereafter, volcanic tremors that occurred in relation to the eruptive activities in Aso Volcano were interpreted on the basis of these four classifications (e.g., Shima 1958; Kubotera 1974). The precise hypocenters of the short-period volcanic tremors (except "the 2nd kind") were not obtained because of the strong heterogeneity of the geological structure around various craters; however, by using tripartite observations, Yoshikawa and Kitunezaki (1959) and Kikuchi (1962) found that the epicenters of the short-period volcanic tremors occur near the first crater.

Eruption earthquakes were studied using the seismograms of the explosive activity in 1933 (Sassa 1935). Although the observations were conducted at only three points, the explosion earthquake included the directions of the initial motion, which suggests a different mechanism than an isotropic mechanism. The tension along the direction that intersects perpendicularly with a crater line (north-northeast–south-southwest) was estimated by using the direction of the initial motion of the stations.

A-type earthquakes (i.e., volcano–tectonic earthquakes) are observed several times per month during the calm activity period. The source region is deeper than sea level at approximately 1 km southeast of the first crater. When the volcanic activity level increases (e.g., the Strombolian eruption stage), the source region of the A-type earthquakes changes to the shallow region beneath the first crater (Ono and Hoka 1984).

In recent years, studies investigating long-period volcanic tremors (including "the second kind" of tremors) have advanced rapidly because of the application of broadband seismometers. Seismic observations conducted using broadband seismometers near the volcano were started in the 1990s: a LPT was found at Aso Volcano with a period exceeding 10 s (Kawakatsu et al. 1994). Very long-period displacements (>100 s) were observed just before a phreatic explosion (Kaneshima et al. 1996), and a long-period volcanic tremor

(LPT) with a dominant period of approximately 15 s and a duration of less than 1 min was also observed (Kawakatsu et al. 2000). These sources are estimated to be a few hundred meters southwest or west of the first crater at depths of 1–1.5 km. These source mechanisms are estimated to be mainly isotropic mechanisms with a minor deviatoric component demonstrated by a moment tensor analysis (Legrand et al. 2000).

Although the volcanic activity stage was calm after 1995, short-period volcanic tremors (isolated or continuous types) and LPTs always occurred at Aso Volcano. By using a dense broadband seismic network (24 stations) installed around the first crater, the spatial variation of the observed signal amplitudes revealed that the source of the LPTs consists of an isotropic expansion and an inflation of an inclined tensile crack with a strike almost parallel to the chain of the craters (Yamamoto et al. 1999a). In contrast, the source mechanism of the short-period volcanic tremors has not been estimated yet because their magnitudes were small, and the volcanic edifices had strong heterogeneities.

After 1995, during a calm activity period, two types of volcanic tremors—isolated- and continuous-type tremors—were observed at Aso Volcano. The latter type has been a subject of research, which continues from Sassa (1935). The continuous tremors have been continually observed in seismic stations around the first crater, although the maximum amplitudes and dominant frequencies change with

the activity stages. The maximum amplitudes of this tremor with dominant frequencies ranging from approximately 3 to 10 Hz are dependent on the volcanic activity stage, and its source region is near the first crater (Takagi et al. 2006). On the one hand, the duration of the isolated tremors is several seconds; they were observed more than 200 times per day, but their magnitudes are much smaller than those of volcanic earthquakes (Japan Meteorological Agency 2005). The waveform characteristic of the isolated tremors changed in 1997. The isolated tremors, which were observed after 1997, have two dominant frequencies—low and high; they were observed almost simultaneously with the LPTs. The isolated tremors with such wave properties were typically short-period volcanic tremors occurring during the calm activity period at Aso Volcano. It is important to clarify the source mechanisms of the isolated tremors to understand the flow system of volcanic fluids during the calm activity period.

Observations

In addition to the permanent seismic stations operated by the Aso Volcanological Laboratory (AVL), Kyoto University, we performed temporary seismic observations in the west rim of the first crater (KAR) to clarify the waveform characteristic of the short-period volcanic tremors from 1995 to 1998 (Fig. 1). However, the number of stations was
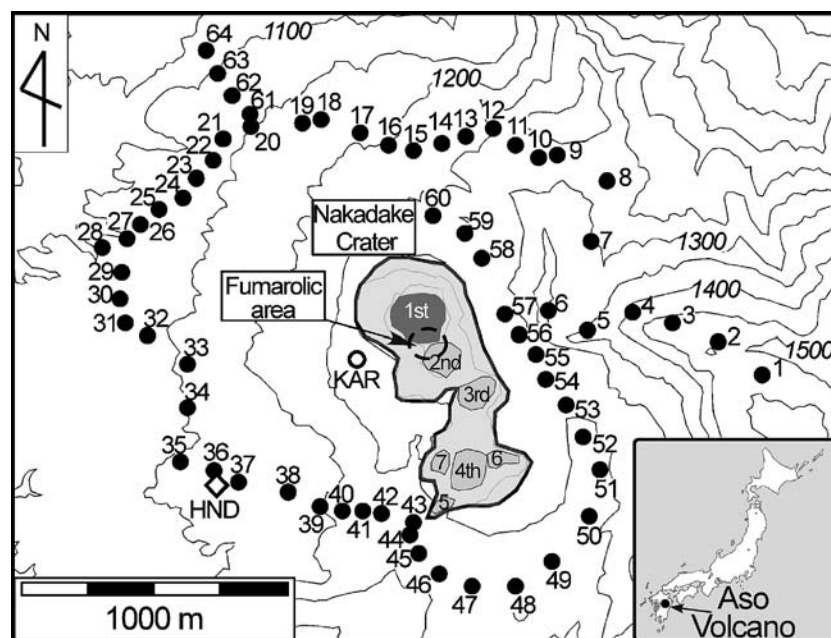
Fig. 1 Location of Aso Volcano and a topographic map of the location around Nakadake crater. Nakadake crater comprises seven craters, and only the first crater has been active in recent years. The first crater has been in the state of a crater lake after 1994. *Diamond* (HND), *open circle* (KAR), and *solid circles* (1–64) show the locations of the seismic stations. The stations denoted by the *solid* *circles* were set by the seismic exploration project at Aso Volcano on November 26, 1998 (Project ASO98). KAR operated from 1995 to 1998, and HND is a permanent station operated by the Aso Volcanological Laboratory, Kyoto University. At the HND, a broadband seismometer (CMG 3) is set inside an observation tunnel at a depth of 30 m

insufficient for estimating the hypocenters of the isolated tremors. The seismic experiment ASO98 was performed to reveal the seismic velocity structure in the central cone of Aso Volcano; it was carried out in November 1998 as part of the Fifth National Project for the Prediction of Volcanic Eruptions (Sudo et al. 2002). Furthermore, 296 temporary stations with vertical-component seismographs were deployed over the central cone of Aso Volcano; 64 temporary stations were deployed near Nakadake crater, which is an active crater (Fig. 1; Tsutsui and Sudo 2004). The number of seismic stations set around Nakadake crater for the ASO98 experiment involves the maximum density of observations performed until now. As detailed observations of the short-period volcanic tremors necessitate many stations near the source region, seismograms obtained by the ASO98 experiment were used in this study.

In the ASO98 experiment, L-22D (Mark Products) seismometers with a natural frequency of 2 Hz and LS-8000SH (Hakusan) data loggers with a 16-bit data resolution were used as the seismometers and recorders, respectively. At all the stations, the sampling frequency of the recorders was 250 Hz, and the recording data were filtered with a 60-Hz low-pass filter installed inside LS-8000SH. Seismograms were recorded from 1 to 5 A.M., and a record time of approximately 2 min was repeated at intervals of approximately 5 min. The seismograms of artificial earthquakes produced by six shots were included in these data sets (Tsutsui and Sudo 2004).

The AVL operates the Hondo observation tunnel (HND) at a location approximately 1 km southwest of the first crater (Fig. 1). In 1995, a broadband seismometer (Guralp CMG-3T) was installed at a depth of 30 m at the HND. Continuous observations were performed at a sampling frequency of 20 Hz for investigating the long-period volcanic tremor.

Characteristics of isolated tremors

Seismograms operated during the ASO98 experiment recorded several isolated tremors (Fig. 2). The magnitudes of these isolated tremors were variable, and the peak-to-peak velocity amplitudes were less than 10 μm/s. Furthermore, the maximum amplitudes of only 18 isolated tremors exceeded twice the amplitude level of the continuous tremor (i.e., background noise) at station 57. The recorded isolated tremors consist of a high-frequency part (HF-part) and low-frequency part (LF-part), and the HF-part always arrived earlier than the LF-part. The dominant frequencies of HF- and LF-parts were approximately 10 and 2 Hz, respectively (Fig. 3). In addition, a 20-Hz peak, which corresponds to the second overtone of the harmonic oscillation with a fundamental mode of 10 Hz, exists in both these spectra (Fig. 3b and c). The existence of this overtone suggests that the oscillation of a resonator is the source of the HF-part.

The dominant frequencies of the other isolated tremors were similar to the result of HB1 and HB2; however, the amplitude ratios of the HF-part to the LF-part were variable. For example, in HB1, the amplitude of the LF-part is greater than the HF-part; on the other hand, in HB2, the amplitude of the HF-part is greater than that of the LF-part (Fig. 3a). As observed during the ASO98 experiment, the time lag of the arrival time between HF- and LF-parts was less than 2 s.

Isolated tremors observed in the ASO98 experiment were consistent with the data recorded after 1997 when the activity level decreased. The time lags of the arrival times of 92 isolated tremors observed at KAR from 1997 to 1998 were also less than 2 s (Fig. 4). Therefore, the isolated tremors observed during the ASO98 experiment can be considered as typical short-period volcanic tremors at Aso Volcano during the calm volcanic activity period. In this

Fig. 2 Example of velocity seismograms observed at station 56. Isolated tremors are observed during continuous tremors. HB1, HB2, and HB3 denote the events that are discussed in detail in the text
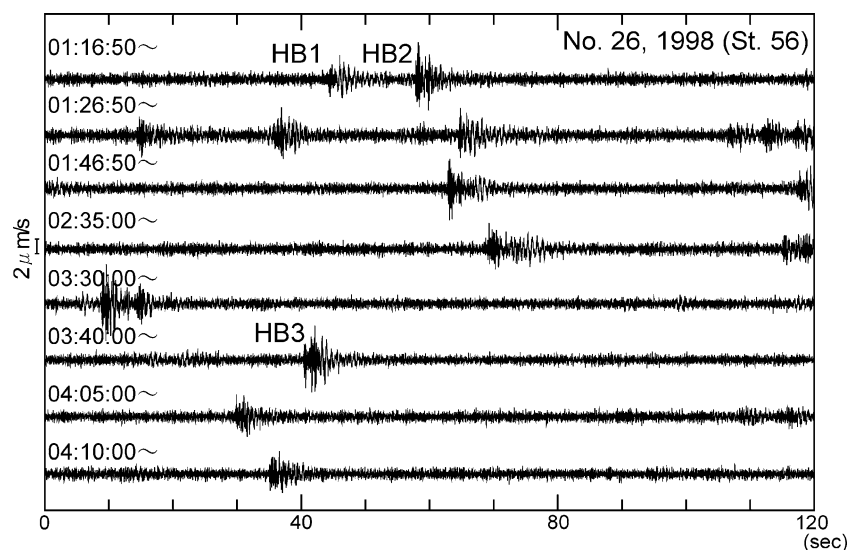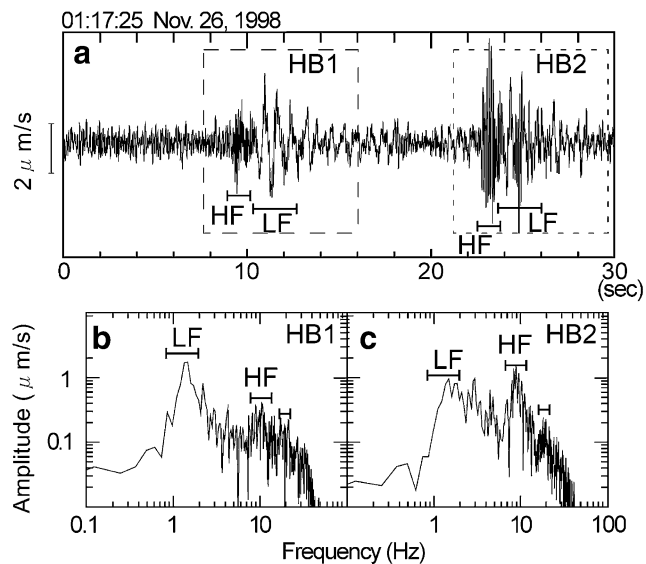
Fig. 3 Example of velocity seismograms and spectra obtained at station 56. **a** Seismograms of two isolated tremors (HB1 and HB2; Fig. 2). **b** Spectrum of HB1 calculated in the time window represented by the broken line. **c** Spectrum of HB2 calculated in the time window shown by the *dotted line*. For the spectra of both HB1 and HB2, the low-frequency part (LF-part) and high-frequency part (HF-part) exhibit peaks at approximately 2 and 10 Hz, respectively. The peak at approximately 20 Hz corresponds to the second overtone of the harmonic oscillation with a fundamental mode of 10 Hz

paper, such isolated tremors with a hybridization waveform characteristic, which include HF- and LF-parts, are called hybrid tremors (HBTs).

Although the HF- and LF-parts in HBTs can be clearly classified in the seismograms obtained near the first crater, HF-parts of the seismograms obtained at stations distant from the crater are not clear (Fig. 5a). The RMS amplitude distribution shows that the HF-part has a large amplitude only at the stations near the first crater, and the station with the maximum RMS amplitude was at station 56 located at the southeastern rim of the crater (Fig. 5b). The RMS
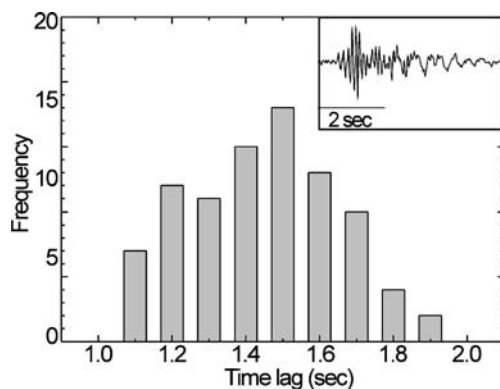
Fig. 4 Seismogram of an isolated tremor observed at KAR in December 1997 and a histogram of the time lags between the HF- and LF-parts for 92 isolated tremors observed at KAR after 1997. Time lags between the HF- and LF-parts range from 1 to 2 s

amplitude distribution suggests that the hypocenter of the HF-part is located in a shallow region beneath the first crater if the major source parameter assumes an isotropic source. In contrast, the RMS amplitude of the LF-part is large at the stations near the first crater similar to the HF-part, but it is also large at the stations in the northwest and southwest regions of the first crater (Fig. 5b). The epicenter of the LF-part is also likely to be near the first crater because station 55 has the maximum RMS amplitude; however, the difference in the RMS amplitude distributions of LF- and HF-parts suggests that the source parameters of the LF-part may be different from the HF-part. In addition, the phases of the LF-part differ between the stations on the eastern side (55–60) and the northwestern side (16–19) of the first crater (Fig. 6). The initial phase is dilatation or pull on the eastern side (55–58), but this phase is not clear on the northern side (59 and 60); this phase is reversed (compression or push) on the northern to the northwestern side (16–19). The characteristic of these initial phases suggests that the source parameter of the LF-part is not purely isotropic.

Source parameters of HBT

RMS amplitude distributions, spectra, and waveform characteristics suggest that the HF- and LF-parts constituting the HBT have different source parameters. Therefore, the source parameters of the HF- and LF-parts need to be separately estimated.
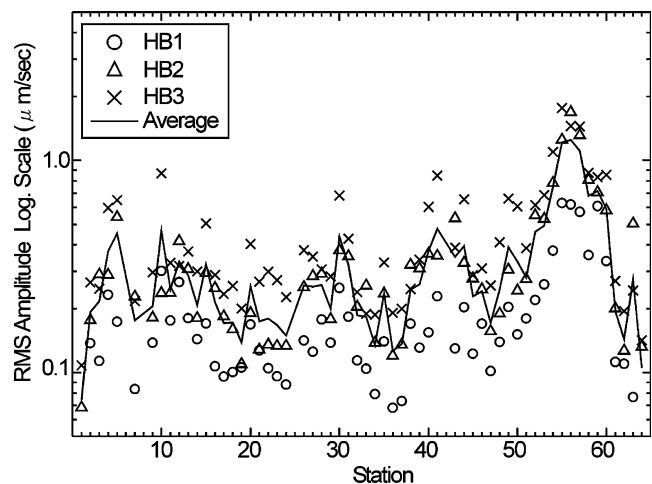
HF-part

It was impossible to estimate the source parameter of the HF-part by using the observed data obtained before the ASO98 experiment was conducted because the magnitude of the HF-part is very small, and the high dominant frequency is strongly influenced by the heterogeneous structure of the volcanic edifice. By using the dense network of seismic stations employed in the ASO98 experiment, we have recorded the waveform of the HF-part in many stations near the first crater, although clear seismograms of the HF-part were obtained only at the station near the first crater even while using the observational data obtained from the ASO98 experiment (Fig. 5). Therefore, we used the amplitude distributions and not the travel times for estimating the source parameters of the HF-part. The RMS amplitude distributions of HF-parts on HB1, HB2, HB3 (Fig. 2), and the average of 13 events (including HB1, HB2, and HB3) have almost the same trends (Fig. 7). These amplitude distributions suggest that HF-parts observed during the ASO98 experiment have the same source parameters.

Fig. 5 Example of HBT seismograms and RMS amplitude ratio distributions. **a** Comparisons of seismograms of an HBT recorded by 19 stations. Seismograms for 15 s including event HB1. **b** RMS amplitude ratio distributions of the HF-part (*top*) and LF-part (*bottom*) of event HB1 plotted on the map of the station network. The RMS amplitudes of the HF- and LF-parts were obtained by filtering the seismograms (**a**) with 5-Hz high-pass and low-pass filters, respectively. The calculated time window for the RMS amplitude is 15 s, as shown in (**a**). The circle's diameter is proportional to the scale of the RMS amplitude ratio. The station with the maximum RMS amplitude is the standard station for obtaining the RMS amplitude ratios. The standard stations of the HF- and LF-parts are stations 56 and 57, respectively
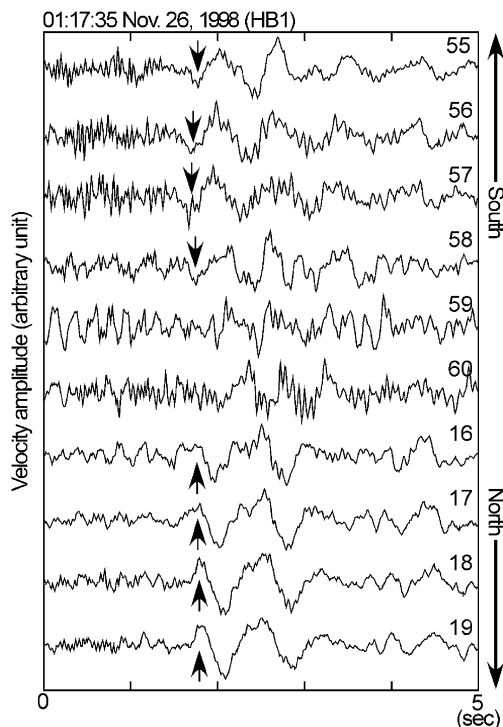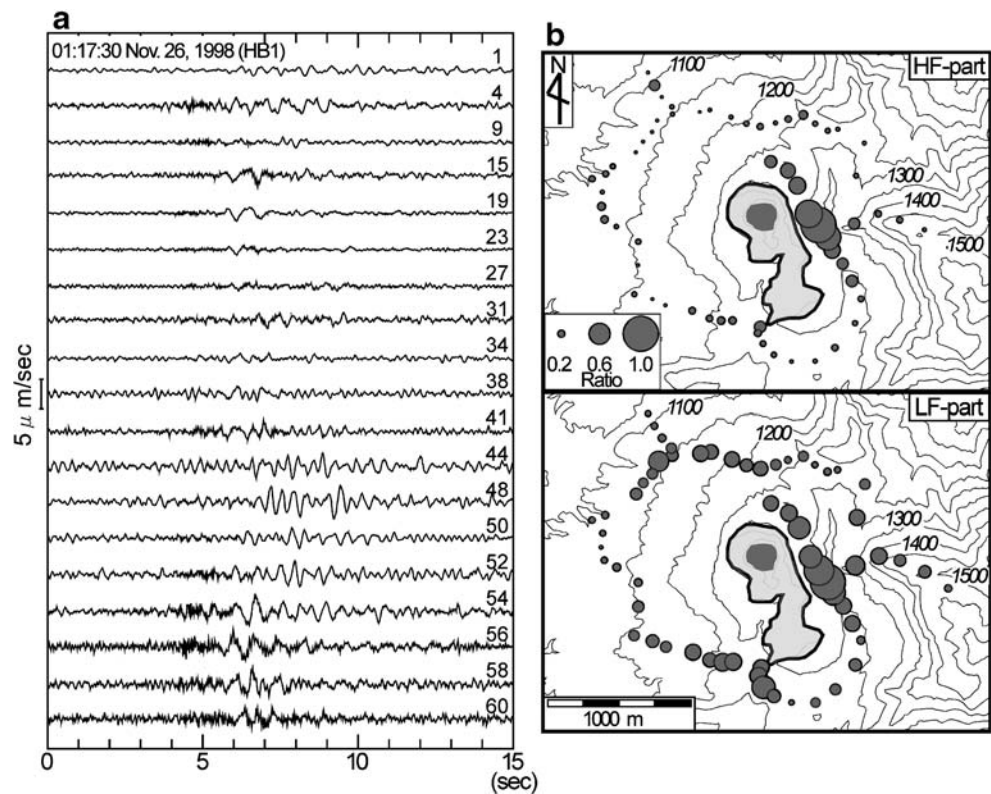
Fig. 6 Comparison of the seismograms of event HB1 observed at stations from the southern to the northern region of the first crater. The top seismogram is obtained at the southernmost station and the bottom seismogram, at the northernmost station. *Arrows* indicate the initial phase of the LF-part. The up-and-down direction of the initial phase changes with the regions, and the seismograms at stations 59 and 60 do not have clear initial phases
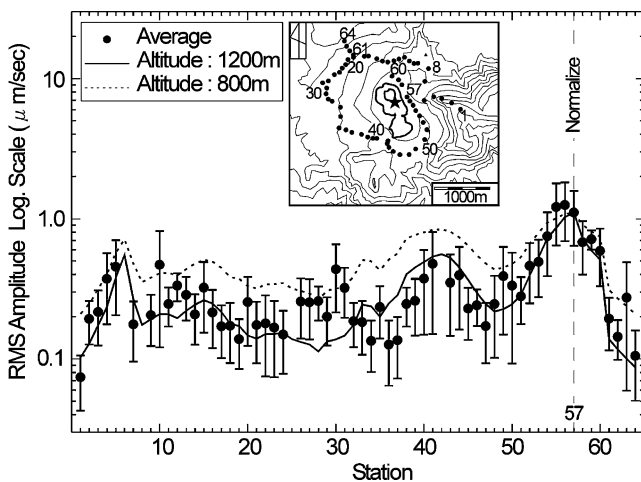
Next, we assumed the main component of the source parameters to estimate the hypocenter of HF-parts by using these amplitude distributions. The result of the spectral analysis showed that the HF-part has two spectral peaks—the fundamental mode and an overtone mode (Fig. 3). An overtone mode can be made by the volume fluctuation
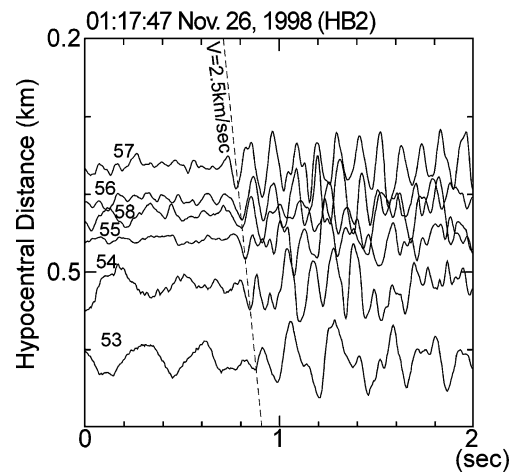

Fig. 7 Amplitude distributions of the HF-part of HB1, HB2, HB3, and the average. RMS amplitude of the HF-part is obtained by filtering the HBTs with a 5-Hz high-pass filter. The time window used for the calculation of the RMS amplitudes is 2 s such that only the HF-part is included. The average is calculated by using the RMS amplitudes obtained for all the 13 events including HB1, HB2, and HB3

inside a structure like a resonator (e.g., Fujita et al. 1995). Although we did not have detailed data regarding the structure of the resonator, the resonator was assumed to be spherical for simplicity. The hypocenter of the HF-part was estimated by comparing the theoretical amplitude distribution, which assumed various hypocentral depths and an isotropic source parameter, and the RMS amplitude distribution. The epicenter was assumed to be to the south of the first crater, where the most active fumarolic area in Aso Volcano is located (Fig. 1). The reason for having assumed this region as the epicenter is that this region is close to the stations with large amplitudes (stations 55, 56, and 57) and has the highest possibility that volume fluctuations will occur. Assuming that the epicenter is located near the active fumarolic area, the theoretical RMS amplitude distributions of the various hypocentral depths, which were assumed at the altitude intervals of 100 m from 0 to 1,200 m, were calculated (Fig. 8). A comparison of the observed and calculated RMS amplitude distributions indicated that the hypocentral depth is close to the active fumarolic area, which is located at an altitude of approximately 1,200 m (Fig. 8). The source region of HF-parts is suggested to be near the surface beneath the fumarolic area.

Next, we verified the reliability of the hypocenter location by comparing the arrival time of the initial phases, which were recorded at the stations close to the first crater (Fig. 9). Even for the station near the first crater, the initial phases of almost all the observed HF-parts were not clear. The HF-part of only HB2 was useful in the comparison. Hypocentral distances at each station are the distances from the
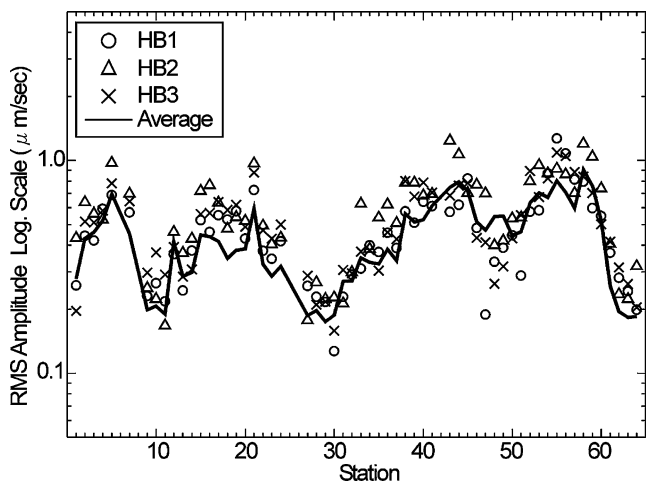

Fig. 9 Seismograms of the initial motion of the HF-part (HB2) at the stations near the first crater. Waveforms are plotted by using the hypocentral distances. The hypocenter is located at an altitude of 1,200 m and denoted by the *star* in the map shown in Fig. 8. The *broken line* with V=2.5 km/s connects the initial phases

hypocenter of the HF-part obtained from the RMS amplitude distribution. When the observed waveforms of the HF-part are plotted in proportion to the hypocentral distances, the initial phases of the HF-part is along the same line. The gradient of this line is 2.5 km/s—nearly equal to the P wave velocity of the shallow region of the first crater obtained by Tsutsui and Sudo (2004). The reliability of the hypocenter of the HF-part estimated by the RMS amplitude distribution is improved for this result. In addition, this reveals that the most active fumarole area at the first crater is the source region of the HF-part, suggesting that the occurrence of the HF-part is related to the fumarolic activity.

LF-part

The RMS amplitude distributions of LF-parts on HB1, HB2, HB3, and the average of 13 events (including HB1, HB2, and HB3) have almost the same trends (Fig. 10): this similarity is better than the amplitude distributions of HF-parts. A similarity of the amplitude distribution suggests that LF-parts have a common source parameter. Furthermore, it is considered that the source parameter of the LF-part differs from that of the HF-part because the large amplitude region of the LF-part differs from that of the HF-part. However, these differences may have been caused by the sensitiveness of the heterogeneous structure. As the wavelength of the LF-part is five times greater than that of the HF-part, the influences of the attenuation and scattering effects induced by the geological structure on the LF-part are lower those on the HF-part. However, we are opposed to the hypothesis that the HF- and LF-parts have the same source parameters, and the difference in the RMS amplitude distribution is caused by a heterogeneous structure. This is because the amplitude distributions have some differences

Fig. 8 Distributions of the average RMS amplitude of the HF-part and theoretical amplitudes. *Error bars* indicate the range of the RMS amplitude values from the 13 HF-parts at each station. The epicenter is assumed to be located in the active fumarolic area (*star*) for calculation of the theoretical amplitude. The results of the theoretical amplitude distributions with a hypocentral depth of 1,200 m above sea level and 800 m above sea level are shown by the *thin and dotted lines*, respectively. The theoretical amplitudes of all the stations were normalized by the amplitude of station 57

Fig. 10 Amplitude distributions of the LF-part of HB1, HB2, HB3, and the average. RMS amplitude of the LF-part is obtained by filtering the HBTs with a 5-Hz low-pass filter. The time window used for the calculation of the RMS amplitudes is 2 s such that only the LF-part is included. The average is calculated using the RMS amplitudes obtained for all the 13 events including HB1, HB2, and HB3

that contradict the assumption that the source parameters are the same. One reason is that the stations with the maximum amplitude differ at the HF- and LF-parts (Fig. 5b). The station that has the maximum amplitude at LF-parts is located to the south of the station recording the HF-part. In addition, in the regions of station 10 (north of the first crater) or station 30 (west of the first crater), the maximum amplitude of HF-parts is greater than the maximum amplitude of LF-parts (see Figs. 5b, 7, and 10). Therefore, we estimate the source parameter of the LF-part independently from that of the HF-part.

For determining the source parameters, we need to clarify the waveform properties (body waves or surface waves) of the LF-part. We attempt to analyze the slowness vector by using the waveform semblance method on the basis of the waveforms of the LF-part with a high SN ratio at the stations northwest of the crater. This method is based on the semblance method (Neidel and Tarner 1971), which has been extensively used to locate either seismic events or point scatterers (e.g., Kuwahara et al. 1997; Kawakatsu et al. 2000). It measures the coherency among the seismograms as follows:

$$S = \frac{\sum_{j=1}^{L} \left(\sum_{i=1}^{N} u_{i,j(i)} \right)^2}{N \sum_{j=1}^{L} \sum_{i=1}^{N} u_{i,j(i)}^2}, \tag{1}$$

where N is the number of stations, $u_{i,j(i)} \equiv u_{i,(t_i + j\Delta t)}$ is a seismogram of the ith station at the $j(i)$th time sample, and L is the number of time samples that defines the time window. The start time $t(i)$ is shifted for each station, depending on the assumed slowness vector of the traversing plane wave or

source distance. Although the LF-part has a more distinct waveform than the HF-part, only several events of LF-parts have a high SN ratio. For the waveform semblance analysis, we selected LF-parts with a high SN ratio (Fig. 11), and selected stations (18, 19, 20, 21, 22, 23, 61, 62, and 63) north–northwest of the crater as the seismic array (Fig. 1). The slowness and incidence azimuth were assumed to be unknown parameters, and those parameter values with the maximum semblance value were searched using a grid search. In HB1, a clear phase appears near 35.7 s, and the semblance value is 0.90 (Fig. 11). The incidence azimuth and slowness were N 146° E and 0.28 s/km (3.6 km/s), respectively. As the P wave velocity at an altitude of 700 m near the crater is estimated to be approximately 3.5 km/s by Tsutsui and Sudo (2004), the phase starting at 35.7 s is considered to be a P wave. The incidence azimuth points toward the direction of the first crater. The result that the hypocenter of the LF-part is along the direction of the first crater is consistent with the result that a large amplitude is recorded at the eastern side of the first crater. After the arrival of the P wave, the waveform changes slightly at 36.2 s, and
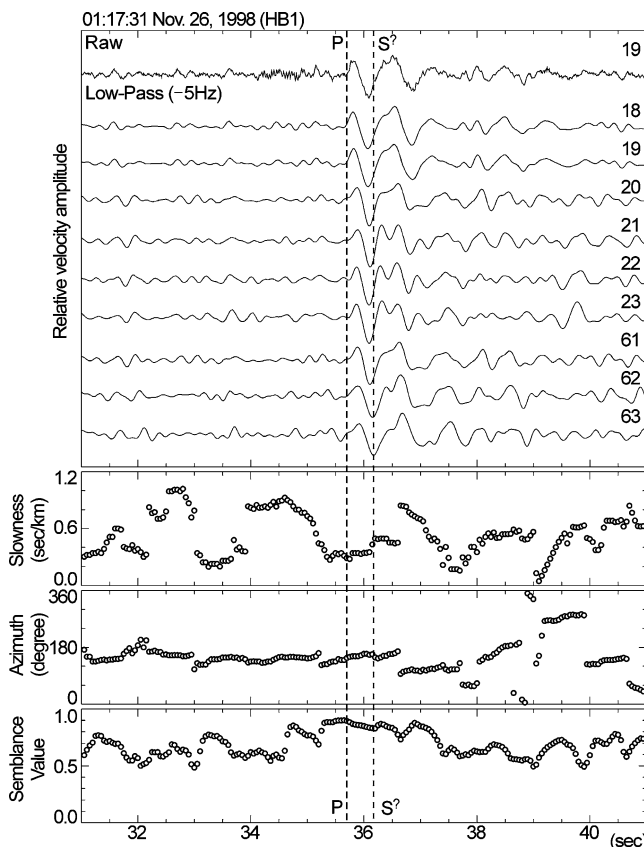
Fig. 11 Results of the semblance analysis for the LF-part (HB1). Semblance analysis is calculated by using the seismograms at stations 18, 19, 20, 21, 22, 23, 61, 62, and 63. Seismograms are filtered by using a 5-Hz low-pass filter. The time window for semblance analysis is 0.5 s, and the moving time window is 0.05 s

the incidence azimuth is along the direction of the first crater (N 148 E), which is similar to the P wave, but the slowness (0.49 s/km) is approximately 1.75 times as large as that of the P wave. The slowness, reversed phase, and RMS amplitude distribution (Figs. 6 and 10) suggest that the LF-part has S-wave components. However, it is unknown if an initial motion of the S wave is present at 36.2 s; this is because such initial motion may be included in the initial phase of the P wave if the hypocentral distance is less than approximately 2 km. The existence of the S wave suggests that the source parameter of the LF-part is not a purely isotropic component.

With regard to the azimuth from the crater and the clearness of the initial motion, seven stations (4, 9, 19, 23, 34, 38, and 56) were selected for hypocenter determination (Fig. 12). Although these stations have initial motions clearer than the other stations, the time precision of the arrival times is not high due to the background noise caused by the continuous tremor. Therefore, hypocenter determination using the time of the phase peak for hypocenter evaluation determined from the arrival time was also performed (Fig. 12). The P-wave velocity used for the hypocenter determination is 3.5 km/s, as obtained by Tsutsui and Sudo (2004), and also from the estimate of the semblance analysis (Fig. 11). As the calculations used two sets of time information, these epicenters were determined to be almost at the same location near the first

crater within the limits of the reading error. In addition, the location reliability is improved because the epicenter of the LF-part is along the direction of the incidence azimuth of the P wave calculated from the semblance analysis (Fig. 12). Hypocentral depths were estimated to be approximately 300±200 m (altitude of 900±200 m). The reliability of the hypocenter depth is poor. In earlier studies, as a P-wave velocity greater than 3.5 km/s was not obtained in the shallow region near the crater, it is likely that the hypocentral depth of the LF-part is less than 300 m.
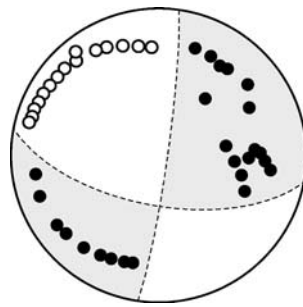
As the distance between the adjacent stations was small, the same phase of the LF-part can be easily identified at every station. Therefore, the source mechanism was estimated using the polarity of the initial phase of HB1 with the largest amplitude (Fig. 13). This result suggests that the dominant component of the source mechanism of the LF-part is a strike–slip component. Polarities were not obtained at the south–southeast region of the first crater. The reason for this phenomenon can be considered to be either the source mechanism of a non-double-couple component or the regional structure of the stony desert; however, this was not evident from the data obtained from the ASO98 experiment. Although the LF-part may have a non-double-couple component, a dominant component of the source mechanism of the LF-part will be a strike–slip component. The pressure axis is along the northeast–southwest direction, if the polarities of the initial motion and the initial phase are the same.
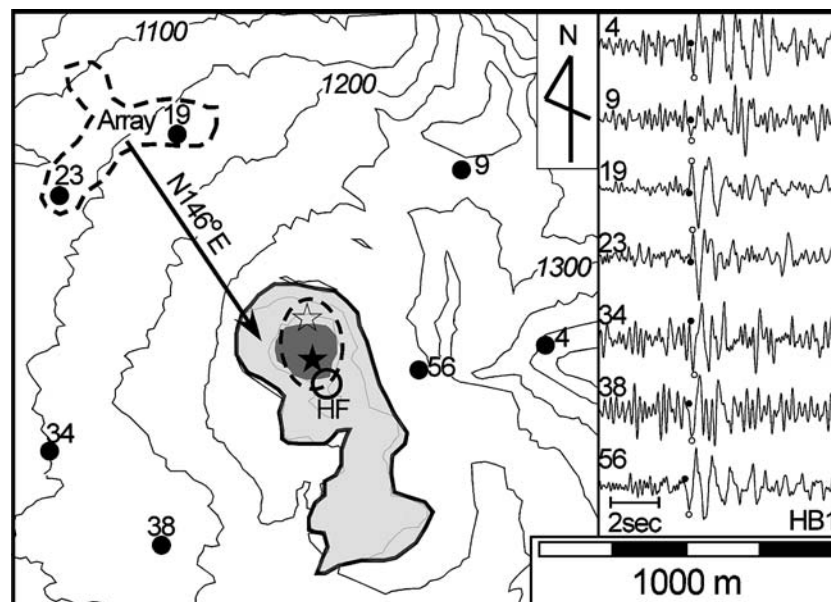
Fig. 12 Hypocentral map of the LF-part (HB1). *Solid circles* are the stations used for the hypocenter determination. The "array" region is the location of the stations used for the semblance analysis shown in Fig. 10, and the arrow indicates the arrival azimuth of the P-wave. The hypocenters are calculated using the arrival times (*solid circles* in the seismograms) and the phase peaks (*open circles* in seismograms). The *solid star* and *open star* denote the locations of the epicenters calculated using the arrival time and the phase peak, respectively. The hypocentral depths were estimated to be approximately 300±200 m (altitude of 900±200 m)

Fig. 13 Focal sphere of the LF-part (HB1). *Solid circles* and *open circles* are the stations with the initial phase of tension (pull) and compression (push), respectively

Fig. 14 Seismograms obtained at the same time at station 57 and HND. Here, the seismometers used are a short-period seismometer (L22D) and a broadband seismometer (CMG3), respectively. The arrival times of the LPT and HF-part (HF) are almost the same and those of the LF-part (LF) are delayed by approximately 1 s
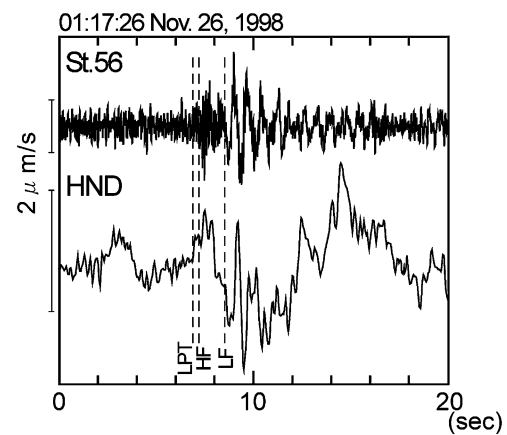
Discussion

From the 18 HBTs observed during the ASO98 experiment, we selected and analyzed 13 HBTs with a high SN ratio to clarify the source parameters. In particular, HB1 (for the LF-part) and HB2 (for the HF-part) for which the SN ratio was the highest among the 13 HBTs were used for the analysis involving the arrival times. As a result, the HF- and LF-parts at the HBT had different source parameters. We estimated that the hypocenters of both HF- and LF-parts occur in the shallow region beneath the fumarole located on the south wall of the first crater and the upper end of the crack (also a source of LPTs), respectively. Each source parameter was common for every event because each amplitude distribution of the HF- and LF-parts was almost the same in every event, implying stable source mechanisms. Although the activity of Aso Volcano after 1997 (when the occurrence of HBTs became clear) was a calm period, the change in the volcanic activity accompanied by the rise in the temperature at the fumarolic area and the rise in the amplitude level of the volcanic tremor (continuous tremor) started in 2000 (Yoshikawa and Sudo 2004). As the volcanic activity was stable from 1997 to 2000, it is considered that HBTs generated during this period were stable and had the same source parameter.

During the activity stage with the occurrence of the HBT, the LPT was also observed. The LPT is constantly observed with the broadband seismometer installed in the HND, regardless of the volcanic activity level of Aso Volcano (Fig. 1). After 1997, the HBT began to appear on the seismogram almost simultaneously with the LPT. In the seismogram including HB1, the LPT and HF-part arrive almost simultaneously, and the LF-part arrives after the LPT and the HF-part (during the oscillation of the LPT; Fig. 14). Almost all the HBTs that were recorded at the HND were accompanied by LPTs with this arrival order.

Yamamoto et al. (1999a) described the LPT as an elastic wave generated by the flow of volcanic fluid inside a crack. They estimated that the size of the fluid-filled crack is 1 km (width) × 2.5 km (depth), and the upper end of the crack has a depth of 300 m beneath the first crater (Fig. 15). The source mechanism of the HF-part is estimated to be a

volume fluctuation in the shallow region beneath the fumarole located on the south wall of the first crater. As the arrival times of the HF-part and the LPT were almost the same, the volume fluctuations at the shallow (under the fumarole) and deep (crack) regions are considered to occur almost simultaneously. To examine the trigger factor that causes the HBT and LPT, the occurrence order of these seismic events assumes the most importance. However, we were unable to compare the origin times of the HF-part and LPT because a high-precision arrival-time determination of the LPT is obstructed by the long-period seismic waves. On the other hand, the occurrence of the LF-part can be attributed to the shear fracture (strike–slip fault) at the upper end of the crack (Fig. 15) within 2 s after the volume fluctuations begin in the crack (LPT). It is already known
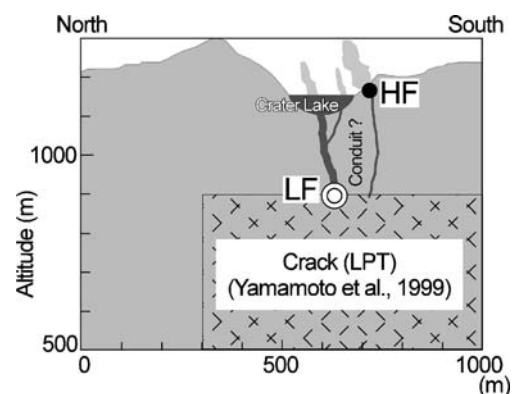
Fig. 15 Schematic illustration of the shallow region in Nakadake crater. Hypocentral locations of the crack (LPT) and the HBT (LF- and HF-parts) are shown. The crack, which is the source of the LPT, has been proposed by Yamamoto et al. (1999a). The hypocenter of the HF-part is estimated to be just under a fumarolic region and is denoted by a *solid circle*. The hypocenter of the LF-part is estimated to be at the upper end of the crack and is denoted by a *double circle*

that a shear fracture occurs with a volume fluctuation. Brace et al. (1966) suggested that a shear fracture occurs with the opening of a crack, and Shimizu et al. (1984) clarified that a shear fracture occurred near the crack by investigating the seismic activity accompanying the 1983 eruption of Miyakejima. The pressure axis (or the tension axis) of the LF-part is nearly perpendicular to the chain of craters, namely, the strike of the crack estimated by Yamamoto et al. (1999a). Thus, it is considered that the shear fracture (strike–slip) of the LF-part occurred because of the closing (or opening) of the crack. In addition, the direction of the pressure axis (or the tension axis) is similar to the direction of the tension axis of the "eruption earthquakes", as determined by Sassa (1935). This similarity suggests that even if the volcanic activity occurs during the calm period, the dominant stress field in the shallow region of Nakadake crater is acting to close (or open) the line of the craters.

It is likely that Nakadake crater with its steady fumarolic activity is forming the steady flow system of the volcanic fluid. This system was also suggested by the results of the self-potential measurements (Hase et al. 2005). We estimated that the isolated tremors with a dominant frequency of a short period, which occurred beneath the steady fumarolic activity, are caused by the volume fluctuations related to the flow of the volcanic fluid. The time relationships between the occurrences of the HBT and LPT are as follows: (1) the volume fluctuation in the shallow region beneath the fumarole (HF-part) and the volume fluctuation inside the crack (LPT) occur almost simultaneously and (2) a shear fracture (LF-part) occurs in the upper end of the crack within 2 s after the occurrence of the volume fluctuations (HF-part and LPT). Although we were unable to estimate the starting point of the volume fluctuation, it is considered that the volume fluctuation (inflation or deflation) inside the crack, or the shallow region beneath the fumarole, triggers the HBT and LPT. The fluctuation in the volcanic plume accompanying these volume fluctuations is not obtained at the present stage; however, to clarify the flow processes of the volcanic fluid in the shallow region of Nakadake crater, pictures and seismograms should be compared with a high-time precision.

Conclusions

The source parameters of isolated hybrid tremors (HBT) were estimated using the data obtained from the ASO98 experiment. This type of tremor was observed starting in Aso Volcano from 1997 when the volcanic activity was calm. The HBT was classified into two parts on the basis of the characteristic frequency: the HF-part with a dominant frequency of approximately 10 Hz and the LF-part with a

dominant frequency of approximately 2 Hz. The hypocenter region of HF-parts was a shallow region beneath the fumarolic area: the major source factor was the volume fluctuation. The LF-part occurred within 2 s after the occurrence of the HF-part. Its hypocenter was at a depth of approximately 300 m beneath the first crater: a strike–slip component was the major component of the source parameters. The HBT and LPT—whose major source parameter is a volume fluctuation inside a crack—occurred almost simultaneously. The hypocentral depth of the LF-part agrees with the depth of the upper end of the crack, which is a source of the LPT. In addition, the HBT and LPT occurred almost at the same time; in particular, the initial motion of the HF-part and LPT is almost the same. As the volume fluctuation was included in the hypocenter parameters of both the tremors, it is obvious that volcanic fluids beneath the active crater are involved in the occurrence of both HBT and LPT. We are certain that the volcanic fluid is related to the occurrence factor of volcanic tremors; the next step is to clarify the flow system of the volcanic fluid in the shallow region beneath Nakadake crater.

References

Brace WF, Paulding BW, Scholz C (1966) Dilatancy in the fracture of crystalline rocks. J Geophys Res 71:3939–3953

Chouet B, Saccorotti G, Dawson P, Martini M, Scarpa R, DeLuca G, Milana G, Cattaneo M (1999) Broadband measurements of the sources of explosions at Stromboli Volcano, Italy. J Geophys Res 102:15129–15150

Fujita E, Ida Y, Oikawa J (1995) Eigen oscillation of a fluid sphere and source mechanism of harmonic volcanic tremor. J Volcanol Geotherm Res 69:365–378

Hase H, Hashimoto T, Sakanaka S, Kanda W, Tanaka Y (2005) Hydrothermal system beneath Aso volcano as inferred from self-potential mapping and resistivity structure. J Volcanol Geotherm Res 143:259–277

Hurst AW (1992) Stochastic simulation of volcanic tremor from Ruapehu. J Volcanol Geotherm Res 51:185–198

Japan Meteorological Agency (2005) National catalogue of the active volcanoes in Japan (Third edition). Japan Meteorological Agency, pp 1–635, (in Japanese)

Kaneshima S, Kawakatsu H, Matsubayashi H, Sudo Y, Tsutsui T, Ohminato T, Ito H, Uhira K, Yamasato H, Oikawa J, Takeo M,

Iidaka T (1996) Mechanism of phreatic eruptions at Aso volcano inferred from near-field broadband seismic observations. Science 273:642–645

Kawakatsu H, Ohminato T, Ito H, Kuwahara Y (1992) Broadband seismic observation at Sakurajima Volcano, Japan. Geophys Res Lett 19:1959–1962

Kawakatsu H, Ohminato T, Ito H (1994) 10s period volcanic tremors observed over a wide area in southwestern Japan. Geophys Res Lett 21:1963–1966

Kawakatsu H, Kaneshima S, Matsubayashi H, Ohminato T, Sudo Y, Tsutsui T, Uhira K, Yamasato H, Ito H, Legrand D (2000) Aso94: Aso seismic observation with broadband instruments. J Volcanol Geotherm Res 101:129–154

Kikuchi S (1962) On the short period volcanic micro-tremors at Mt. Aso. Bull Volcanol Soc Jpn 7:1–16, (in Japanese)

Kubotera A (1974) In: Civetta L, Gasparini P, Luongo G, Rapolla A (eds) Volcanic tremors at Aso volcano. Physical Volcanology, Elsevier, pp 29–47

Kuwahara Y, Itoh H, Kawakatsu H, Ohminato T, Kiguchi T (1997) Crustal heterogeneity as inferred from seismic coda wave decomposition by small-aperture array observation. Phys Earth Planet Inter 104:247–256

Legrand D, Kaneshima S, Kawakatsu H (2000) Moment tensor analysis of near-field broadband waveforms observed at Aso Volcano, Japan. J Volcanol Geotherm Res 101:155–169

Miller AD, Stewart RC, White RA, Luckett R, Baptie BJ, Aspinall WP, Latchman JL, Lynch LL, Voight B (1998) Seismicity associated with dome growth and collapse at the Soufriere Hills Volcano, Montserrat. Geophys Res Lett 25:3401–3404

Mori T, Notsu K (1997) Remote CO, COS, CO_2, SO_2, HCl detection and temperature estimation of volcanic gas. Geophys Res Lett 24:2047–2050

Mori T, Mori T, Kazahaya K, Ohwada M, Hirabayashi J, Yoshikawa S (2006) Effect of UV scattering on SO_2 emission rate measurements. Geophys Res Lett 33:L17315

Neidel N, Tarner MT (1971) Semblance and other coherency measures for multichannel data. Geophysics 36:483–497

Ono H, Hoka T (1984) Seismic activity near the Nakadake, Volcano Aso in 1981. Joint Geophysical and Geochemical Observations of Aso Volcano: 7–16, (in Japanese)

Ono K, Watanabe K (1985) Geological map of Volcanoes 4; Geological map of Aso Volcano 1: 50000. Geological survey of Japan, Tsukuba, (in Japanese)

Sassa K (1935) Volcanic micro-tremors and eruption-earthquakes (part 1 of the geophysical studies on the Volcano Aso). Mem Coll Sci Kyoto Univ 18:255–293

Seidl D, Kirbani SB, Brüstle W (1990) Maximum entropy spectral analysis of volcanic tremor using data from Etna (Sicily) and Merapi (central Java). Bull Volcanol 52:460–474

Shima M (1958) On the second volcanic micro-tremor at the Volcano Aso. Disaster Prevent Res Inst Kyoto Univ Bull 22:1–6

Shimizu H, Ueki S, Koyama J, Takagi A (1984) Mechanisms of volcanic earthquakes following the 1983 eruption of Miyakejima. Bull Volcanol Soc Jpn 29:S81–S100, (in Japanese)

Sudo Y, 89 persons (2002) 1998 seismic exploration, Aso98, in Aso Volcano. Bull Earthq Res Inst 77:303–336

Takagi N, Kaneshima S, Kawakatsu H, Yamamoto M, Sudo Y, Ohkura T, Yoshikawa S, Mori T (2006) Apparent migration of tremor source synchronized with the change in the tremor amplitude observed at Aso volcano, Japan. J Volcanol Geotherm Res 154:181–200

Tanaka Y (1994) Eruption mechanism as inferred from geomagnetic changes with special attention to the 1989–1990 activity of Aso Volcano. J Volcanol Geotherm Res 56:319–338

Tsutsui T, Sudo Y (2004) Seismic reflectors beneath the central cones of Aso Volcano, Kyushu, Japan. J Volcanol Geotherm Res 131:33–58

Yamamoto M, Kawakatsu H, Kaneshima S, Mori T, Tsutsui T, Sudo Y, Morita Y (1999a) Detection of a crack-like conduit beneath the active crater at Aso Volcano, Japan. Geophys Res Lett 26:3677–3680

Yamamoto M, Kawakatsu H, Kaneshima S, Iidaka T, Oikawa J, Watada S, Morita Y, Mori T, Tsutsui T, Sudo Y, Yoshikawa S, Hashimoto T, Nakaboh M (1999b) ASOBOI97: Aso Seismic Observation with Broadband Instruments in 1997. Bulletin of the Earthquake Research Institute 74:267–285

Yoshikawa S, Kitsunezaki C (1959) On the short period volcanic micro-tremors at volcano Aso. Bull Volcanol Soc Jpn 3:147–153, (in Japanese)

Yoshikawa S, Sudo Y (2004) Volcanic activity and surface temperature variation of crater lake in Naka-dake crater at Aso volcano. Annuals of Disas Prev Res Inst Kyoto Univ 47:803–807, (in Japanese)